A Log-Likelihood Fit for Extracting Muon Neutrino Oscillation Parameters

Xuheng Zhao

***Abstract*—The neutrino oscillation parameters were extracted from the simulated T2K experimental data. The method of uncertainty estimation was examined using a 1D parabolic minimiser, and six minimisation methods were discussed by carrying out 2D minimisation on a known function and then on the problem. Wolfe condition was examined throughout. However, the expected distribution using the resulted parameters failed to agree with the observed, motivating a 3D minimisation. The parameters obtained were $\hat{\theta} = 0.7529$ rad, $\Delta\hat{m}^2_{23} = 2.513 \times 10^{-3}$ eV^2, and $\hat{\alpha} = 1.295$ GeV^{-1} with percentage uncertainties less than 5%. The results were confirmed as the global minimum using two simulated annealing methods. Hypothesis testing was conducted to confirm the agreement between the observed and expected distributions.**

I. Introduction

As neutrinos travel, they vary between the three flavors (i.e. electron, ν_e, muon, ν_μ, and tau, ν_τ neutrinos) via neutrino oscillations [1]. This phenomenon is only possible if neutrinos have a non-zero mass, and the first experiment that best measured the relevant parameters was the T2K experiment [2]. To replicate the process of extracting the oscillation parameters, the observed neutrino events before and after the neutrino oscillation were simulated and regenerated, as shown in Fig. 1. minimisation methods and statistical techniques were then applied.

II. Theory

A. Neutrino oscillations

The first-order approximation to the 'survival probability' of ν_μ is expressed as

$$P_{(\nu_\mu \to \nu_\mu)} = 1 - \sin^2(2\theta_{23}) \sin^2\left(\frac{1.267 \Delta m^2_{23} L}{E_{\nu_\mu}}\right), \tag{1}$$

where θ_{23} is the ν_μ-ν_τ 'mixing angle', Δm^2_{23} is the difference between the squared masses of ν_μ and ν_τ in eV^2, L is the distance traveled by ν_μ in km, and E_{ν_μ} is the ν_μ energy in GeV [1]. The 'survival probability' is plotted as shown in Fig. 2, where neutrino oscillations mainly occur in the low energy region.

B. Statistics of functional minimisation

Since only $\mathcal{O}(100)$ neutrino events were observed as shown in Fig. 1, the probability density function $\mathcal{P}(\vec{u}; m_i)$ in each bin can be modeled by a Poisson distribution,

$$\mathcal{P}(\vec{u}; m_i) = \frac{\lambda_i^{m_i}(\vec{u})\ e^{-\lambda_i(\vec{u})}}{m_i!}\ , \tag{2}$$

where λ_i and m_i are the expected and observed number of entries in bin i respectively, and $\vec{u}$ is a set of parameters that govern λ_i [1]. To estimate $\vec{u}$ that gives the best agreement between the observed and simulated distributions, the combined likelihood function for n numbers of independent measurements m_i,

$$\mathcal{L}(u) = \prod_{i=1}^{n} \mathcal{P}(\vec{u}; m_i)\ , \tag{3}$$

is maximised [1]. However, functional minimisation is much easier to achieve. Thus, the negative log-likelihood, or NLL, of a Poisson distribution,

$$NLL(\vec{u}) = 2\sum_{i=1}^{n} \left[\lambda_i(\vec{u}) - m_i \ln(\lambda_i(\vec{u})) + \ln(m_i!)\right], \tag{4}$$

will be minimised to obtain the best set of $\vec{u}$ [1].

Combining with (1), $\lambda_i(\vec{u})$ can be calculated by

$$\lambda_i(\vec{u}) = k_i \cdot P_{(\nu_\mu \to \nu_\mu)}\ , \tag{5}$$

where k_i is the initially unoscillated entries in bin i, and (1) suggests that $\vec{u} = (\theta_{23}, \Delta m^2_{23})$ [1]. NLL is periodic every $\theta_{23} = \pi/2$ and symmetric with respect to $\theta_{23} = \pi/4$ due to the $\sin^2$ term in (1). One can easily verify that if Δm^2_{23} is not within $[1.00, 4.00] \times 10^{-3}$, $P_{(\nu_\mu \to \nu_\mu)}$ is insignificant. Thus, the first global minimum (i.e., the minimum with

the smallest θ_{23}) is within $\theta_{23} \in [0.6, \pi/4]$ and $\Delta m^2_{23} \in [1.00, 4.00] \times 10^{-3}$. The units of the values are dropped for conciseness.

In addition, considering the neutrino interaction cross-section that is proportional to the energy at each bin center $\bar{E}_{\nu_\mu}$, (5) is modified as

$$\lambda_i(\vec{u}) = k_i \cdot P_{(\nu_\mu \to \nu_\mu)} \cdot \alpha \cdot \bar{E}_{\nu_\mu} \ , \qquad (6)$$

where α is a proportionality constant, and $\vec{u} = (\theta_{23}, \Delta m^2_{23}, \alpha)$ [1].

By minimising NLL to NLL_{min} to estimate the best $\vec{u}$, $\hat{\vec{u}}$, the uncertainty of $\hat{\vec{u}}$, $\sigma_{\hat{\vec{u}}}$, corresponds to the change of the absolute unit of 1 around $NLL(\hat{\vec{u}})$ (i.e. NLL_{min}) [3], [4], which means $\sigma_{\hat{\vec{u}}}$ can be solved from

$$NLL(\hat{\vec{u}} \pm \sigma_{\hat{\vec{u}}}) - (NLL_{\text{min}} + 1) = 0 \ . \qquad (7)$$

Although (7) is derived from the NLL of a Gaussian distribution, it still remains valid for non-Gaussian likelihoods with a large n [4]. The $\sigma_{\hat{\vec{u}}}$ can also be obtained from the square root of the diagonal elements of the covariance matrix [4], which is the inverse of a Hessian matrix $\mathbf{H}$ [5].

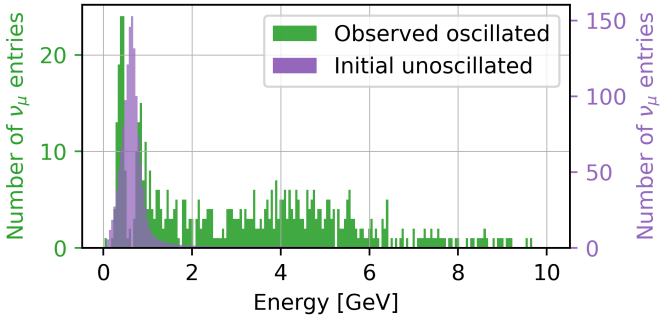

Fig. 1: Histogram showing the observed oscillated and initially unoscillated ν_μ data with the peak entries aligned. Both sets of data were randomly simulated according to the T2K experiment [1].

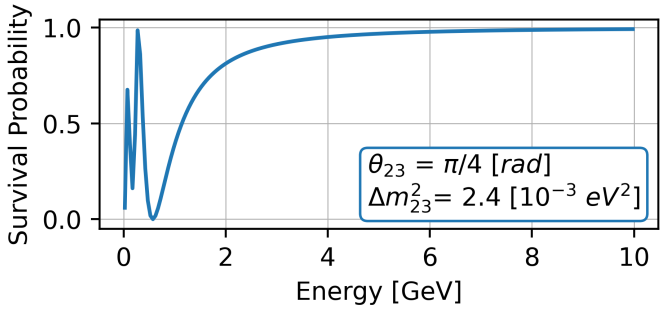

Fig. 2: Plot of $P_{(\nu_\mu \to \nu_\mu)}$ against E_{ν_μ}. The θ_{23} and Δm^2_{23} values used in (1) are annotated. The neutrino oscillations, represented by the fluctuations of the curve, are mostly within the 1 GeV range of E_{ν_μ}.

III. One-dimensional minimisation

To examine the methods of uncertainty estimation, a one-dimensional minimisation was carried out by substituting (5) into (4) with $\Delta m^2_{23} = 2.4 \times 10^{-3}$. From direct observation of Fig. 3, NLL is decreasing monotonically before reaching the first minimum, and thus, a parabolic minimiser was used. All results and uncertainties are shown in Table I.

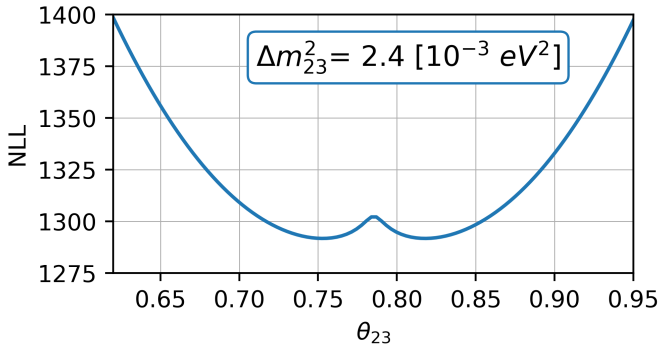

Fig. 3: Plot of NLL against θ_{23} with Δm^2_{23} fixed. The first NLL_{min} is around $\theta_{23} = 0.75$. Any iteration steps must not exceed $\theta_{23} = \pi/4$, which is a local maximum or the axis of symmetry

A. Parabolic minimiser

Three initial guesses less than $\theta_{23} = \pi/4$ (i.e. the axis of symmetry) were taken around the minimum to avoid inaccurate calculations if the points around the next minima were involved. A parabola was interpolated, in which the minimum x_3 was calculated with the 2nd-order Lagrange polynomial [3],

$$x_3 = \frac{1}{2} \frac{(x_2^2 - x_1^2)y_0 + (x_0^2 - x_2^2)y_1 + (x_1^2 - x_0^2)y_2}{(x_2 - x_1)y_0 + (x_0 - x_2)y_1 + (x_1 - x_0)y_2} \ . \qquad (8)$$

The largest point among x_0, x_1, x_2 was substituted by x_3, and this process was repeated until the stopping condition was reached, which means the absolute change of NLL between subsequent iterations was less than 10^{-10}.

B. Uncertainty estimation

To estimate $\sigma_{\hat{\theta}_{23}}$, (7) was solved using the secant method with each iteration updated as [3]

$$x_{j+1} = x_j - f(x_j) \frac{x_j - x_{j-1}}{f(x_j) - f(x_{j-1})} \ . \qquad (9)$$

Two initial guesses were used to estimate $\sigma_{\hat{\theta}_{23}}$ on either side of $\hat{\theta}_{23}$. The stopping condition of 10^{-10}

was used, and the $\pm\sigma_{\hat{\theta}_{23}}$ obtained were slightly different on either side of $\hat{\theta}_{23}$ as expected [4].

The $\sigma_{\hat{\theta}_{23}}$ was also obtained from the covariance matrix of size 1×1, where the central difference scheme to the 2nd-order accuracy,

$$\frac{df}{dx} \approx \frac{f(x+h) - f(x-h)}{2h} \ , \tag{10}$$

was used for computing the first-order derivatives [3]. The step size h was calculated by scaling x with the machine epsilon of float32 (i.e. in the magnitude of 10^{-7}), which was not too large to give significant truncation errors and not too small to give underflow on the numerator, resulting a zero gradient otherwise. The second-order derivatives in $\mathbf{H}$ were computed by differentiating the first-order derivatives again with (10), which kept the truncation error in $\mathcal{O}(h^2)$.

TABLE I: Results of 1D minimisation

$\hat{\theta}_{23}$ [rad]	$\sigma_{\hat{\theta}_{23}}$ [rad]	
1D Parabolic	$NLL_{\text{min}} + 1$	Covariance matrix
0.7529	$+0.0110$ -0.0120	± 0.0116

Both of the methods gave $\sigma_{\hat{\theta}_{23}} \approx 1.5\%$, confirming the robustness of the values. Although the covariance matrix cannot capture the asymmetry around NLL_{min}, it is still favored as it is not affected by the choice of initial guesses, unlike the secant method, and can obtain the uncertainty with much less computation power while ensuring accuracy.

IV. Two-dimensional minimisation and comparison of methods

To compare different minimisation methods, a two-dimensional minimisation was carried out by substituting (5) into (4), which both θ_{23} and Δm^2_{23} are the free parameters. The same stopping condition of 10^{-10} was used for all methods except the two simulated annealing ones. All methods were tested on a known function before applied, the details can be found in the code submitted. The paths taken for each method are shown in Fig. 4, and the results and uncertainties are listed in Table II.

A. Comparison of methods

The simplest multidimensional minimiser, the univariate method, was used, which is the parabolic minimiser applied to each parameter direction successively [3]. As long as the correct initial guess was applied, it was a very stable method and could always converge to the global minimum without any modifications of the method's internal parameters, unlike some of the methods below.

Simultaneous minimisation methods were used next. Starting with the simplest gradient descent method, each iteration was calculated from

$$\vec{x}_{j+1} = \vec{x}_j - \alpha_j \nabla f(\vec{x}_j) \ , \tag{11}$$

where ∇f is the gradient [3]. The Armijo rule of the Wolfe condition,

$$f(\vec{x}_{j+1}) = f(\vec{x}_j + \alpha_j \vec{p}_j) \leq f(\vec{x}_j) + c\alpha_j \vec{p}_j{}^T \nabla f(\vec{x}_j) \ , \tag{12}$$

was examined in each iteration, where α_j is a constant that controls the step length, $\vec{p}_j$ is the search direction for the best $\vec{x}_{j+1}$, and c is a scaling constant which 10^{-4} is used [6]. In each iteration, α_j was reset to its initial guess and scaled depending on (12). If (12) was satisfied, $\vec{x}_{j+1}$ would be accepted, and the iterations continued. Otherwise, α_j was halved, and this process was repeated. Since the gradient along Δm^2_{23} is significantly larger than that along θ_{23}, the α_j along Δm^2_{23} was scaled to be 10^{-5} smaller so that each step was roughly perpendicular to the contour.

To avoid potential problems due to a poor choice of α_j, Newton's method was used, where the iterations were updated according to [3]

$$x_{j+1} = x_j - \mathbf{H}^{-1} \nabla f(\vec{x}_j) \ , \tag{13}$$

where $\mathbf{H}$ was obtained as described in *Uncertainty estimation* section. $\mathbf{H}$ must be positive definite to ensure convergence to a minimum rather than a maximum or saddle point [3], which suggests that the initial guesses must be at a location with a concave curvature.

To avoid $\mathbf{H}$ being non-positive, the quasi-Newton method was used, in which $\mathbf{H}^{-1}$ in (13) was approximated with an update matrix $\mathbf{G}_j$ as

$$x_{j+1} = x_j - \alpha_j \mathbf{G}_j \nabla f(\vec{x}_j) \ , \tag{14}$$

where α_j is a scaling constant [3]. In the first iteration, $\mathbf{G}_0$ was set to an identity matrix and

updated later according to the Davidon-Fletcher-Powell algorithm of [3]

$$\mathbf{G}_{j+1} = \mathbf{G}_j + \frac{(\vec{\delta} \otimes \vec{\delta})}{\vec{\gamma}_j \cdot \vec{\delta}_j} - \frac{\mathbf{G}_j \cdot (\vec{\gamma}_j \otimes \vec{\gamma}_j) \cdot \mathbf{G}_j}{\vec{\gamma}_j \cdot \mathbf{G}_j \cdot \vec{\gamma}_j} \ , \quad (15)$$

where

$$\vec{\delta_j} = x_{j+1} - x_j \text{ and } \vec{\gamma_j} = \nabla f(\vec{x}_{j+1}) - \nabla f(\vec{x}_j) \ . \quad (16)$$

For each iteration, α_j was reset to 1 to ensure quick convergence, but it was halved successively if (12) was not satisfied.

The four methods mentioned above all required a good choice of initial guesses, for which simulated annealing was applied to ensure the results obtained were at the global minimum.

Two types of annealing methods, classical simulated annealing (CSA) and fast simulated annealing (FSA), with the Metropolis Algorithm were used [3]. In each iteration, θ_{23} and Δm^2_{23} were updated by adding a random value scaled by their current magnitude [3]. The random value was obtained from a visiting function, which was Gaussian for CSA and Lorentzian for FSA [7], [8]. The acceptance probability was

$$p_{acc} = \begin{cases} 1 & \Delta E \leq 0 \\ \exp(-\Delta E / k_B T) & \Delta E > 0 \ , \end{cases} \quad (17)$$

where ΔE represented the change in NLL, T was the artificial temperature, and k_B = 1 [3]. The value of T was decreased from its initial value according to

$$T = \rho \ T_0 \ , \quad (18)$$

where ρ was between 0 and 1, for CSA [7], and

$$T = \frac{T_0}{j} \ , \quad (19)$$

where j was the number of iterations starting from 1, for FSA [8]. With $T_0 = 80$, both CSA and FSA were run 10 times with 8000 and 4000 iterations each to avoid that some trials may not converge to the global minimum. Fewer iterations were used for FSA because both the faster T decrement and the higher probability of obtaining a large random number from the Lorentzian distribution suggested that FSA could find the global minimum quicker and was less likely to diverge away from the global minimum. The distribution of the accepted steps for all 10 runs of CSA and FSA were plotted into a histogram as shown in Fig. 5, and a Gaussian was fitted to estimate $\hat{\theta}_{23}$ and $\Delta\hat{m}^2_{23}$.

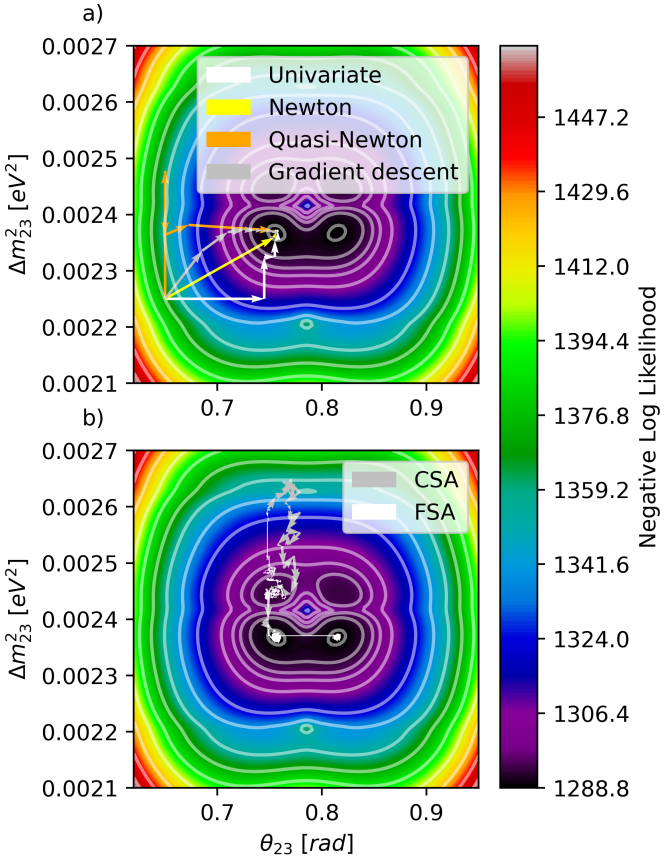

Fig. 4: Plots of the path taken for each method. a) Univariate and the three simultaneous minimisation methods. The same initial guesses were used, and all methods converged to the same point. The oscillations of the first two steps of the Quasi-Newton method were due to the significant difference between the θ_{23} and the Δm^2_{23} gradient. b) The accepted steps of the two simulated annealing methods. FSA moved with larger steps and thus was more likely to step between two global minima.

B. Results and discussions

The uncertainties of $\hat{\theta}_{23}$ and $\Delta\hat{m}^2_{23}$, $\sigma_{\hat{\theta}_{23}}$ and $\sigma_{\Delta\hat{m}^2_{23}}$, were estimated using the covariance matrix. The uncertainties of $\hat{\theta}_{23}$ and $\Delta\hat{m}^2_{23}$ obtained from Gaussian fits, as shown in Fig. 5, were roughly or less than 0.1% for both CSA and FSA. These values were insignificant compared to $\sigma_{\hat{\theta}_{23}}$ and $\sigma_{\Delta\hat{m}^2_{23}}$, which were roughly 1%, as shown in Table II.

The first four methods gave exactly the same results since the stopping condition of 10^{-10} was used for all, which means the values are the same

when keeping only four significant figures. Since the Hessian was calculated according to the magnitudes of $\hat{\theta}_{23}$ and $\Delta\hat{m}^2_{23}$, $\sigma_{\hat{\theta}_{23}}$ and $\sigma_{\Delta\hat{m}^2_{23}}$ would be the same as well. As θ_{23} and Δm^2_{23} were sampled randomly in the two annealing methods, the $\hat{\theta}_{23}$ and $\Delta\hat{m}^2_{23}$ values would be slightly deviated from the global minimum but still precise enough to confirm that the global minimum was found using the first four methods.

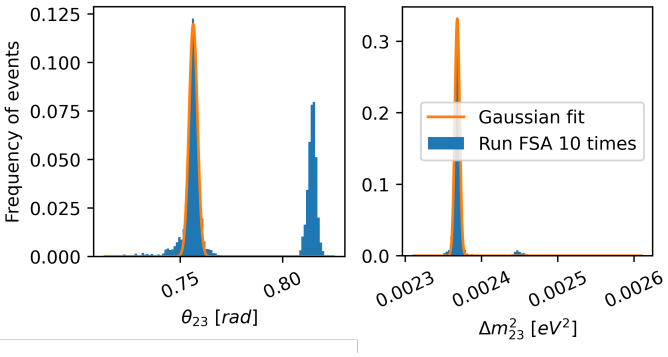

Fig. 5: Histograms showing the distribution of the accepted steps and the Gaussian fits for θ_{23} on the LHS and Δm^2_{23} on the RHS after running FSA 10 times with 4000 iterations each. The histograms for CSA were very similar but with more 'noise' around the peaks, as expected from Fig. 4 (b). The peak around $\theta_{23} = 0.81$ was from the neighboring global minimum, and the small peak around $\Delta m^2_{23} = 2.45 \times 10^{-3}$ was from the local minimum.

TABLE II: Results of 2D minimisation

Methods	$\hat{\theta}_{23} \pm \sigma_{\hat{\theta}_{23}}$ [rad]	$\Delta\hat{m}^2_{23} \pm \sigma_{\Delta\hat{m}^2_{23}}$ [$\times 10^{-3}$ eV^2]
Univariate	0.7562 ± 0.0133	2.368 ± 0.022
Gradient Descent	0.7562 ± 0.0133	2.368 ± 0.022
Newton	0.7562 ± 0.0133	2.368 ± 0.022
Quasi-Newton	0.7562 ± 0.0133	2.368 ± 0.022
CSA	0.7554 ± 0.0132	2.369 ± 0.022
FSA	0.7561 ± 0.0133	2.368 ± 0.022

By substituting $\hat{\theta}_{23} = 0.7562$ and $\Delta\hat{m}^2_{23} = 2.368 \times 10^{-3}$ into (5), an updated version of Fig. 1 is plotted as shown in Fig. 6.

Due to the low number of entries (i.e. less than five) in each bin for both the observed and expected histograms in Fig. 6, a modified chi-squared test was employed to assess their agreement. The chi-squared obtained for each bin was divided by the William's correction factor,

$$q = 1 + \frac{n^2 - 1}{6N\nu} \ , \tag{20}$$

where n is the number of bins, N is the total sample size, and ν is the degrees of freedom [9]. With the modified reduced chi-squared $\chi^2_{\text{red}} = 10.61$ and 198 degrees of freedom, an overflow was encountered when calculating the p-value, suggesting that it was less than 1×10^{-16}. For a null hypothesis that 'the observed and expected distributions are in agreement within a 0.05 significance level', it was rejected since $p < 0.05$. This was expected by direct observation of Fig. 6, and consequently, a better expected distribution should be found.

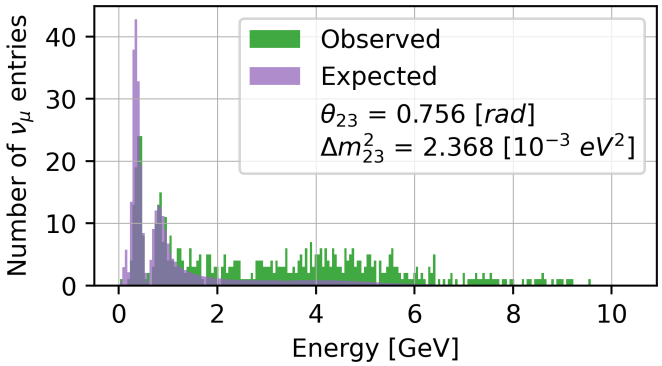

Fig. 6: Histogram showing the observed and expected oscillated entries of ν_μ with the $\hat{\theta}_{23}$ and $\Delta\hat{m}^2_{23}$ values annotated. The observed and expected data were poorly agreed for $E_{\nu_\mu} > 2$ GeV.

V. Three-dimensional minimisation

A. Methods and results

Substituting (6) into (4), where θ_{23}, Δm^2_{23}, and α are all the free parameters, NLL_{min} was estimated again. The results and uncertainties are all listed in Table III. Since it was difficult to visualise the NLL function with three free parameters, FSA was run 10 times to quickly find NLL_{min}. This result was also confirmed by CSA, where the slow decrement of T in Equation (18) compared to Equation (19) suggested that it could search for a longer time and thus be less likely to miss the true global minimum. The precise position of the global minimum was estimated with the other four methods, where the initial guesses of $\theta_{23} = 0.7$, $\Delta m^2_{23} = 2.5 \times 10^{-3}$, and $\alpha = 1.2$ were used. The uncertainties of $\sigma_{\hat{\theta}_{23}}$,

$\sigma_{\Delta\hat{m}^2_{23}}$, and $\sigma_{\hat{\alpha}}$ were all obtained from the covariance matrix.

TABLE III: Results of 3D minimisation

Methods	$\hat{\theta}_{23}$ $\pm\sigma_{\hat{\theta}_{23}}$ [rad]	$\Delta\hat{m}^2_{23}$ $\pm\sigma_{\Delta\hat{m}^2_{23}}$ [$\times 10^{-3}$ eV^2]	$\hat{\alpha}$ $\pm\sigma_{\hat{\alpha}}$ [GeV^{-1}]
Univariate	0.7529 ±0.0213	2.513 ±0.026	1.295 ±0.056
Gradient Descent	0.7528 ±0.0213	2.513 ±0.026	1.295 ±0.056
Newton	0.7529 ±0.0213	2.513 ±0.026	1.295 ±0.056
Quasi-Newton	0.7529 ±0.0213	2.513 ±0.026	1.295 ±0.056
CSA	0.7541 ±0.0218	2.512 ±0.026	1.296 ±0.056
FSA	0.7530 ±0.0214	2.513 ±0.026	1.295 ±0.056

B. Discussions

The values of $\hat{\theta}_{23}$, $\Delta\hat{m}^2_{23}$, and $\hat{\alpha}$ for the two annealing methods were the same within two significant figures, and the precise values were given by the last four methods. The percentage uncertainties of the values were no more than 5%, confirming their accuracy. Substituting $\hat{\theta} = 0.7529$, $\Delta\hat{m}^2_{23} = 2.513 \times 10^{-3}$, and $\hat{\alpha} = 1.295$ into (6), Fig. 6 was updated as Fig. 7.

The modified reduced chi-squared with 197 degree of freedom were calculated again as $\chi^2_{\text{red}} = 0.77$, and the same hypothesis testing was carried out as described in the *Two-dimensional minimisation* section. The p-value obtained was $p = 0.99$, which $p > 0.05$, suggesting that it was failed to reject the null hypothesis with 0.05 significance level. Thus, the observed and expected distributions agreed with each other, suggesting the accuracy of the $\hat{\theta}_{23}$, $\Delta\hat{m}^2_{23}$, and $\hat{\alpha}$ values.

VI. Conclusion

The simulated T2K observed oscillated and initially unoscillated data underwent 1D, 2D, and 3D minimisation. Uncertainty estimation was examined through a 1D parabolic minimiser, yielding NLL_{min} with $\hat{\theta}_{23} = 0.7529 \pm 0.0116$ rad. The univariate and three simultaneous minimisation methods were compared in 2D minimisation, where Wolfe condition was assessed. The global minimum of $\hat{\theta}_{23} = 0.7562$ rad and $\Delta\hat{m}^2_{23} = 2.368 \times 10^{-3}$ eV^2 found by these four methods was confirmed by two simulated annealing methods. All methods were tested on a known function before applied. However, the histogram of observed and expected distribution did not agree, motivating 3D minimisation. The new NLL_{min} was found at $\hat{\theta} = 0.7529$ rad, $\Delta\hat{m}^2_{23} = 2.513 \times 10^{-3}$ eV^2, and $\hat{\alpha} = 1.295$ GeV^{-1} with percentage uncertainties less than 5%, and was also confirmed using two annealing methods. The agreement between observed and expected distributions were confirmed via hypothesis testing.

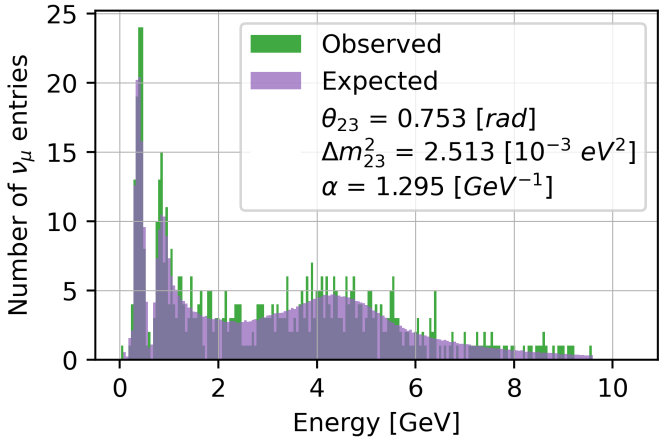

Fig. 7: Histogram showing the observed and expected oscillated entries of ν_μ with the $\hat{\theta}_{23}$, $\Delta\hat{m}^2_{23}$, and $\hat{\alpha}$ values annotated. The observed and expected data were agreed reasonably well.

References

[1] M. Scott and J. Owen, "Project 1: A log-likelihood fit for extracting neutrino oscillation parameters," 2023.

[2] T2K-Collaboration, "Measurements of neutrino oscillation in appearance and disappearance channels by the t2k experiment with 6.6 $\times$ 10^{20} protons on target," *Physical Review D*, vol. 91, no. 7, p. 072010, 2015.

[3] M. Scott and J. Owen, "Computational physics lecture notes," 2023.

[4] M. Richards, "Statistics of measurement lecture notes," 2022.

[5] W. H. Press, S. A. Teukolsky, W. T. Vetterling, and B. P. Flannery, *Numerical Recipes: The Art of Scientific Computing*. Cambridge University Press, 2007.

[6] L. Armijo, "Minimization of functions having lipschitz continuous first partial derivatives," *Pacific Journal of mathematics*, vol. 16, no. 1, pp. 1–3, 1966.

[7] S. Kirkpatrick, C. D. Gelatt Jr, and M. P. Vecchi, "Optimization by simulated annealing," *science*, vol. 220, no. 4598, pp. 671–680, 1983.

[8] H. Szu and R. Hartley, "Fast simulated annealing," *Physics letters A*, vol. 122, no. 3-4, pp. 157–162, 1987.

[9] J. H. McDonald, *Handbook of biolological statistics*. New York, 2014.